

# Controlled Drug Delivery using Functionalized Layered Double Hydroxides for Tumor Treatment



## ABSTRACT

Thesis submitted in partial fulfillment for the  
Award of Degree

**Doctor of Philosophy**

***Swapan Maity***

SCHOOL OF MATERIALS SCIENCE AND TECHNOLOGY  
INDIAN INSTITUTE OF TECHNOLOGY  
(BANARAS HINDU UNIVERSITY)  
VARANASI - 221005  
INDIA

ROLL NO- 19111007

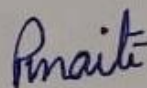
2024



# CERTIFICATE

This is to certify that the thesis entitled "*Controlled Drug Delivery using Functionalized Layered Double Hydroxide for Tumor Treatment*" by *Swapan Maity* has been conducted under my supervision. I confirm that this work is original and has not been submitted elsewhere for the award of any degree. Furthermore, it is certified that the candidate has successfully completed all necessary requirements, including the Comprehensive Examination, Candidacy, and State of the Art (SOTA), for the conferment of the Ph.D. degree.

**Date:** 04.02.2025



**Signature: Supervisor**

**Prof. Pralay Maiti**

**School of Materials Science and Technology**

**IIT BHU (Varanasi)**

Professor/आचार्य

School of Materials Science & Technology/पदार्थ विज्ञान एवं प्रौद्योगिकी स्कूल

Indian Institute of Technology/भारतीय प्रौद्योगिकी संस्थान

(Banaras Hindu University), Varanasi/काशी हिन्दू विश्वविद्यालय, वाराणसी





*Dedicated to*  
*My parents and Family*





## DECLARATION OF THE CANDIDATE

I, Swapan Maity, hereby certify that the work presented in this thesis is my own original and bona fide effort, conducted under the esteemed guidance of Prof. Pralay Maiti from July 2019 to July 2024, at the School of Materials Science & Technology, Indian Institute of Technology (BHU), Varanasi. The content of this thesis has not been submitted for the award of any other degree or diploma.

I declare that due recognition has been given to all research workers whose contributions have been referenced throughout this thesis. I have diligently acknowledged their work and ensured proper citation wherever required. Furthermore, I affirm that I have not deliberately replicated any other individual's work, including paragraphs, texts, data, results, or any material published in journals, books, magazines, reports, dissertations, theses, or accessible through websites, without proper attribution, and I have not presented such material as my own.

Date: 04.02.2025

Signature of the Student

Swapan Maity

Place: Varanasi



## CERTIFICATE BY THE SUPERVISOR

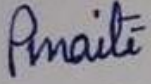
I hereby certify that the above statement provided by the student is accurate and true to the best of my knowledge.

**Supervisor**

**Prof. Pralay Maiti**

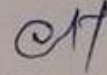
**School of Materials Science & Technology,**

**IIT (BHU), Varanasi**



**Signature of Supervisor**

School of Materials Science & Technology, **मदर्य विज्ञान एवं प्रौद्योगिकी संस्थान**  
Indian Institute of Technology/भारतीय प्रौद्योगिकी संस्थान  
(Banaras Hindu University), Varanasi/काशी हिन्दू विश्वविद्यालय, वाराणसी



**Signature of coordinator**

**Coordinator/समन्वयक**  
School of Materials Science & Technology/मदर्य विज्ञान एवं प्रौद्योगिकी संस्थान  
Indian Institute of Technology/भारतीय प्रौद्योगिकी संस्थान  
(Banaras Hindu University), Varanasi/काशी हिन्दू विश्वविद्यालय, वाराणसी



# COPYRIGHT TRANSFER CERTIFICATE

**Title of the Thesis: "Controlled Drug Delivery using Functionalized Layered Double Hydroxides for Tumor Treatment"**

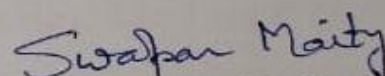
**Name of the student: Swapan Maity**

## Copyright Transfer

The undersigned hereby assigns to the Indian Institute of Technology (Banaras Hindu University), Varanasi, all rights under copyright that may exist in and for the above thesis, submitted in fulfilment of the requirements for the award of the degree of "*Doctor of Philosophy*".

**Date:** 04.02.2025

**Place:** Varanasi

  
Signature of the Student

(Swapan Maity)

**Note:** The author reserves the right to reproduce or grant permission for others to reproduce material taken directly from the thesis, or any derivative works, for personal use. Proper acknowledgment of the source and the Institute's copyright notice must be included in all such reproductions.



## Acknowledgements

First and foremost, I would like to express my heartfelt gratitude to my supervisor **Prof. Pralay Maiti**, Professor, School of Materials Science and technology, IIT (BHU), Varanasi for his wise guidance, affections, continuous interest, and encouragement throughout the research work. All is presented here would not have happened without his scientific vision and constant support. I have spent almost six years in the School of Materials Science and Technology, IIT (BHU), Varanasi. During this period, I have experienced a lot of things which not only help me in further research carrier but also in real life. I feel proud to be a part of this school. I would like to thank all the respected teachers of the school, Prof. Dhananjay Pandey, Prof. Rajiv Prakash, Dr. Chandanan Rath, Dr. Akhilesh Kr. Singh, Dr. Chandan Upadhyay, Dr. Bholanath Pal, Dr. Ashish Kumar Mishra, Dr. Shrawan Mishra, Dr. Sanjay Singh, Dr. Ravi Panwar, Dr. Uday Shankar, Dr. Nikhil Kumar for their valuable suggestions and encouragement during research work. I would like to thank Prof. Biswasjit Ray, Faculty of Science, BHU, Dr. S. Hemalatha Department of Pharmaceutics, IIT (BHU), Dr. Jairam Meena Department of Pharmaceutics, IIT (BHU), Prof. Ram Sharan Singh Department of Chemical Engineering and Technology, IIT (BHU), Dr. Ashish Kumar Agrawal Department of Pharmaceutics, IIT (BHU), Dr. Amrita Ghosh Kar and Dr. Tanima Mandal, Institute of Medical Sciences, Banaras Hindu University, Varanasi and Manas Kumar Santra, National Centre for Cell Science, Pune for providing me necessary instrumental facility along with heartfelt cooperation. Finally, I wish to thank all the labmates and specifically for Souvik Chowdhury, Dipesh Kumar Dubey, Dr. Shivam Tiwari, Dr. Arun Kumar Mahanta, Dr. Aparna Shukla along with my friend Dr. Debadatta Mohapatra, Akshita Upreti and Hitesh Harsukhbhai Chandpa for nice cooperation and enjoyable company. I am also thankful to UGC, New Delhi, India for providing me financial assistantship in the form of JRF and SRF during the research program. I gratefully acknowledge CIF and the Param Shivay Supercomputing Facility IIT (BHU), Varanasi for providing various instrumental facilities. Last but not the least I wish to recall the endless support and love of my family members which inspired me in every step.



# **CONTENTS**

Acknowledgements .....	13
Contents.....	15
Table of Figure .....	21
List of Table .....	35
Abbreviations .....	37
Preface.....	41
<b>Chapter 1: Introduction .....</b>	<b>45</b>
1.1 Background.....	47
1.2 Different mechanisms for controlled drug release .....	49
1.2.1 Diffusion controlled release.....	49
1.2.2 Stimuli controlled release .....	50
1.2.3 Degradation controlled release .....	50
1.2.4 Solvent controlled release.....	50
1.3 Drug delivery systems .....	51
1.3.1 Liposome.....	51
1.3.2 Hydrogel.....	52
1.3.3 Dendrimer .....	53
1.3.4 Micelle .....	54
1.3.5 Polymer.....	55
1.4 Nanoparticles in controlled drug delivery and cancer therapy.....	56
1.4.1 Inorganic nanoparticles.....	57
1.4.2 Organic nanoparticles .....	59
1.4.3 Hybrid nanoparticles .....	60
1.4.4 Targeting Mechanisms.....	61
1.4.5 Targeting endothelial cells.....	62
1.4.6 Overcoming drug resistance mechanisms.....	63
1.4.7 Targeting the Hypoxic Tumor Microenvironment.....	63

1.5	Layered double hydroxide (LDH) Nanoparticles in controlled drug delivery and cancer therapy.....	63
1.5.1.	Structure and Composition of LDH Nanoparticles.....	64
1.5.2	Mechanisms of Drug Delivery.....	65
1.5.3	Targeted Delivery and Biocompatibility.....	66
1.5.4	Overcoming Drug Resistance.....	67
1.5.5.	Future Perspectives.....	67
1.6	Grafted polymers for controlled drug delivery: Focus on polyurethane grafted polymers.....	68
1.6.1	Mechanism and actions.....	68
1.6.2	Polyurethane grafted polymers .....	69
1.6.3	Advantages and future directions .....	69
1.7	Objective of the present thesis.....	71
1.8	Content and scope of the present work.....	72
1.9	References.....	75
<b>Chapter 2 .</b>	<b>Experimental .....</b>	<b>85</b>
2.1	Synthesis of Layered Double Hydroxide and Functionalized Layered Double Hydroxide for sustained drug release.....	87
2.1.1	Materials .....	87
2.1.2	Synthesis of Lithium (Li)-Aluminum (Al) based layered double hydroxides (LDHs)...76	
2.1.3	Design of Drug (Doxorubicin) intercalated Li-Al based LDHs nanoformulation .....	88

2.1.4	Synthesis of polyurethane grafted Lithium (Li)-Aluminum (Al) based layered double hydroxide (LDH) nanocomposite .....	88
2.1.5	Synthesis of the doxorubicin drug intercalated polyurethane grafted Li-Al based LDH nanocomposite system.....	90
2.2	Material Characterizations .....	91
2.2.1	X-ray photoelectron spectroscopy (XPS) .....	91
2.2.2	Particle size and zeta potential (Dynamic Light Scattering, DLS) .....	91
2.2.3	X-ray diffraction (XRD) .....	91
2.2.4	Fourier Transform Infrared Spectroscopy (FTIR) .....	92
2.2.5	UV- Vis Spectroscopy .....	92
2.2.6	Nuclear magnetic resonance (NMR) .....	92
2.2.7	Thermal study .....	92
2.2.8	Mechanical Study.....	93
2.2.9	Morphological investigations.....	93
2.2.10	Brunauer-Emmett-Teller (BET).....	94
2.2.11	Rheological analysis.....	94
2.2.12	Dynamic Mechanical Analysis (DMA).....	94
2.2.13	Computational study.....	95
2.3	<i>In-Vitro</i> Drug release Study.....	96
2.4	Detailed <i>in vitro</i> study.....	96
2.4.1	Cell culture and viability study .....	96
2.4.2	Cell adhesion.....	97
2.4.3	Fluorescence imaging.....	98
2.4.4	Cellular uptake.....	99
2.4.5	Intracellular tracking.....	99
2.4.6	Cell cycle analysis using Flow cytometry.....	100
2.4.7	Analysis of protein expression through Western blotting.....	101
2.5	Animal Studies.....	102

2.5.1. <i>In vivo</i> anti-tumor efficacy.....	102
2.5.2 <i>In vivo</i> biodistribution along with pharmacokinetics study.....	102
2.5.3 Histopathology along with biochemical assessments.....	103
2.5.4 Immunohistochemistry.....	104
2.6 Statistical Analysis.....	105

**Chapter 3 . Doxorubicin Intercalated Li-Al Based LDHs as Potential Drug Delivery Nano-vehicle with pH-responsive Therapeutic Cargo for Tumor ..... 105**

3.1 Introduction.....	107
3.2 Result and discussion.....	112
3.2.1 Evaluation of chemical formula and basic characterizations of the nanocarriers and drug loaded nanocarriers .....	112
3.2.2 Shape, size and properties of the nanocarriers.....	118
3.2.3 Encapsulation and Sustained Release Profile of DOX in Li-Al Based LDHs along with Theoretical Understanding of Interaction.....	121
3.2.4 Biocompatibility of nanocarriers along with <i>in vitro</i> cell killing efficiency of DOX loaded nanovehicles.....	127
3.2.5 Controlled cellular uptake along with LDH nanocarrier induced cell adhesion.....	132
3.2.6 <i>In vitro</i> apoptotic mechanistic pathway using nanoformulation.....	135
3.2.7 Molecular Docking Analysis.....	139

3.2.8	<i>In vivo</i> Tumor Study Using a Melanoma Mouse Model.....	141
3.2.9	Histopathological and Immunohistopathological Analyses.....	145
3.3	Conclusion.....	148
3.4	References.....	150
<b>Chapter 4: Controlled Drug Delivery using Functionalized Layered Double Hydroxides.....</b>		<b>157</b>
4.1	Introduction.....	159
4.2	Results and discussion.....	163
4.2.1	Designing of the tumor targeting polyurethane grafted Li-Al based LDH nanocomposite with thermal stability: Thermal and mechanical responses in graft copolymer.....	163
4.2.2	Morphological understanding of prepolymer grafted Li-Al based LDH nanocomposite.....	175
4.2.3	Mechanical, dynamical, and rheological behavior of the nanocomposite.....	178
4.2.4	Encapsulation and sustained release profile of Dox in Polyurethane grafted Li-Al based LDH nanocomposite.....	186
4.2.5	Theoretical Understanding of Interaction through Thermodynamics and Mechanical Response.....	189
4.3	Conclusion.....	194
4.4	References.....	195
<b>Chapter 5: Thermodynamically Stable Organic Inorganic Hybrid for Drug delivery vehicle to Shrinkage the Melanoma</b>		<b>205</b>
5.1	Introduction.....	207
5.2	Results and discussion.....	208

5.2.1	Biocompatibility and <i>in vitro</i> Cell Killing Efficiency of Dox-Loaded Nanovehicles.....	208
5.2.2	Understanding Controlled Cellular Uptake and Novel Nanocomposite – Induced Cell Adhesion.....	212
5.2.3	Unveiling the Apoptotic Mechanistic Pathway <i>in vitro</i> : Harnessing Novel Formulation for Precision Therapy.....	215
5.2.4	<i>In Vivo</i> Tumor Treatment Using a Luciferase-Containing Melanoma Mouse Model with Pharmacokinetic Analysis.....	221
5.2.5	Histopathological and Immunohistopathological Analyses.....	225
5.3	Conclusion.....	229
5.4	References.....	232
<b>Chapter 6:</b>	<b>Conclusion .....</b>	<b>235</b>
6.1	, Conclusion.....	237
6.2	Plan for future work.....	240
	<b>List of Publications.....</b>	<b>243</b>
	<b>Patent and Conference presentations .....</b>	<b>247</b>

## *Table of figures*

<b>Figure 1.1:</b> A Schematic representations of controlled drug delivery system over conventional one [Bajpai et al., 2008].....	47
<b>Figure 1.2:</b> Different drug delivery systems for cell specific drug delivery [ Singh, A. P., Biswas, A., Shukla, A., & Maiti, P. (2019). Targeted therapy in chronic diseases using nanomaterial-based drug delivery vehicles. <i>Signal transduction and targeted therapy</i> , 4(1), 33.].....	54
<b>Figure 1.3:</b> Nanoparticles (NPs) for cancer therapy encompass various types including organic, inorganic, and hybrid NPs.....	59
<b>Figure 1.4</b> Passive and active targeting of nanoparticles (NPs) to cancer cells enhances therapy efficacy while minimizing systemic toxicity. Passive targeting utilizes the enhanced permeability and retention (EPR) effect, leveraging increased vascular permeability and weakened lymphatic drainage. Active targeting involves ligand-receptor interactions, with receptors on cancer cells including transferrin, folate, glycoproteins, and EGFR[Yao, Y., Zhou, Y., Liu, L., Xu, Y., Chen, Q., Wang, Y., ... & Shao, A. (2020). Nanoparticle-based drug delivery in cancer therapy and its role in overcoming drug resistance. <i>Frontiers in molecular biosciences</i> , 7, 193.].....	61
<b>Figure 1.5:</b> Advantages and biomedical application of LDH .....	64
<b>Figure 1.6:</b> Cancer Treatment by using Dox intercalated Mg-Al based LDH( <i>Journal of Materials Chemistry B</i> , 2018, 6(36), 5768-57743.....)	66
<b>Figure 1.7:</b> Polyurethane grafted materials for controlled drug delivery ( <i>Macromolecules</i> , 48(8), 2654-2666).....	70

**Figure 3.1** Characterizations along with understanding the nature of Li-Al based LDHs nanocarriers. **a)** Comparative XPS spectra for Al 2p (left) and Li 1s (right) in LDH1, LDH2 and LDH3 nanocarriers, interestingly the binding energy value for both Al 2p and Li 1s cases slightly increases from LDH1 to LDH3; **b)** Powder X-ray diffraction patterns of LDH1, LDH2 and LDH3 nanocarriers; **c)** Comparative representation of solid state UV-Vis spectra of different indicated nanocarriers; **d)** FTIR spectra of the nanocarriers, displaying a shift in peak position from LDH1 to LDH3 nanocarriers by increasing the percentage of aluminum; and **e)** DSC thermograms of the indicated nanocarriers mentioning the melting temperature and heat of fusion.....114

**Figure 3.2:** **a)** Powder x-ray diffraction patterns (XRD) of DOX intercalated Li-Al based LDHs nanoformulations named DOX@LDH1 and DOX@LDH3; **b)** XRD data table which reflects the slightly decreasing trend of  $d_{003}$  spacing of (003) plane from LDH1 to LDH3 but crystalline domain size (calculated from Debye-Scherrer equation) gradually increases from LDH1 to LDH3. In the case for DOX intercalated systems i.e. DOX@LDH1 and DOX@LDH3,  $d_{003}$  spacing are equal in both of the cases but crystalline domain size increases from DOX@LDH1 to DOX@LDH3, this is mainly due to the large sized nanocarrier LDH3; **c)** Solid state UV-Vis spectra of DOX, DOX@LDH1 and DOX@LDH3. In case of DOX, the peak arises in 267 nm but when it is incorporated into the nanocarriers LDH1 and LDH3 formed nanoformulation DOX@LDH1 and DOX@LDH3, the peak is shifted to higher wavelength region such as 303 and 292 nm indicating strong interaction between drug molecule and nanocarriers; **d)** FTIR spectra of pristine DOX along with nanoformulations DOX@LDH1 and DOX@LDH3 showing shifting in peak positions due to interactions. The major peak position of drug molecule (DOX) arises in 3333, 1617, 1582  $\text{cm}^{-1}$  which is shifted 3432, 1628, 1586  $\text{cm}^{-1}$  and 3420, 1615, 1583  $\text{cm}^{-1}$  for DOX@LDH1 and DOX@LDH3, respectively; **e)** DSC thermograms of DOX@LDH1 and DOX@LDH3 indicating the melting temperature and heat of fusion values. The melting temperature of pristine DOX is 217°C which is shifted to 168°C in both of the cases. Interestingly, the heat of fusion of DOX@LDH3 is quite high (185.59  $\text{J.g}^{-1}$ ) as compared to the DOX@LDH1 (36.16  $\text{J.g}^{-1}$ ); **f)** TGA thermograms of LDH1, LDH2 and LDH3 nanocarriers with their relative thermal stability. 5 % degradation temperature of LDH1, LDH2 and LDH3 are 168, 185 and 188°C respectively showing higher thermal stability of LDH3 compared to others.....117

**Figure 3.3:** : Size and morphological analysis of different Li-Al based LDH nanocarriers along with their relevant properties, **a)** HRSEM images of LDH1, LDH2 and LDH3 nanocarriers: Size gradually increases from LDH1 to LDH3 with hexagonal morphology. The histogram analysis of the nanocarriers size distribution are shown in the individual inset; **b)** HRTEM microscopic image of hexagonal like morphology with increasing trend of size from LDH1 to LDH3 confirming the results obtained from HRSEM. From LDH1 to LDH3, increasing percentage of aluminum (Al) results towards increasing trend of size; **c)** the hydrodynamic diameter and zeta potential of LDH1, LDH2 and LDH3 nanocarriers were determined using dynamic light scattering (DLS), and justify the results obtained from HRSEM and HRTEM *i.e.* increasing trend of size from LDH1 to LDH3; **d)** AFM images of LDH1, LDH2 and LDH3 ( $3 \times 3 \mu\text{m}^2$ ) measured through semi-contact mode; and **e)** Evaluation of surface area for LDH1, LDH2 and LDH3 nanocarriers indicating large surface Area for smaller size particle.....120

**Figure 3.4:** Size dependency along with pH-triggered drug release features from the designed nanoformulation and strong interaction between DOX and Li-Al based LDHs. **a)** Comparative cumulative drug release profile of DOX loaded LDHs (DOX@LDH1 and DOX@LDH3) in PBS at a particular pH ~7.4 at 37 °C; **b)** Comparative release profiles of DOX from DOX@LDH3 in PBS in various pH media (pH ~7.4, 6 and 4 at 37 °C. Data expressed as mean value  $\pm$ SD (n=3); **c)** Schematic diagram illustrating the release of drugs from different size nanovehicles. Large size nanovehicle (DOX@LDH3) exhibit sustained drug release because of greater confinement and stronger interaction whereas small size nanocarrier (DOX@LDH1) shows a burst release of drug; **d)** Theoretical evaluation of interaction between DOX molecule and different Li-Al based LDHs nanoformulation with increase in doping aluminum (Al) concentration into the lithium hydroxide (LiOH) crystal for representative systems of LiOH+DOX, LiAl1OH+DOX, LiAl2OH+DOX and LiAl3OH+DOX nanoformulations having representing color codes of different atoms: blue-Aluminum, green-Lithium, red-Oxygen, white- Hydrogen, pink-Nitrogen, and black-Carbon; **e)** Variation of total energy of Li-Al based LDHs and DOX loaded LDHs (LDH+DOX) nanoformulations before and after interaction between DOX and different nanocarriers (LiOH, LiAl1OH, LiAl2OH and LiAl3OH);

**f)** Comparative study of total energy of free DOX molecule and DOX molecule intercalated in different Li-Al based LDHs nanocarriers; and **g)** Comparative analyses of closest H-bonded distance between DOX molecule and H- atom in Li-Al based LDHs nanocarriers in different indicated nano formulations.....123

**Figure 3.5:** a) Cumulative release of drug from the indicated specimens showing sustained drug release profile from graft copolymers; b) Schematic model showing the architecture of copolymer and drug which cause sustained release from low graft density copolymer against high graft density copolymer; c) Bar diagram of contact angle of various graft copolymers showing hydrophobic nature of low graft density copolymers as compared to high graft density copolymer ..... 125

**Figure 3.6:** a) Fluorescent microscopic images of AO/ EtBr staining of LDH1, LDH2 and LDH3 nanocarriers; b) Cell viability study of LDH1, LDH2 and LDH3 against SiHa cells using MTT assay as a function of time; c) Cell viability of LDH1, LDH2 and LDH3 nanocarriers against 3T3-L1 using MTT assay as a function of time d) Phase contrast images of LDH1, LDH2 and LDH3 nanocarriers; e) Percentage cell adhesion value of LDH1, LDH2 and LDH3 nanocarriers..... 129

**Figure 3.7:** Comparison study of biocompatibility and *in vitro* cytotoxicity on cancer cell line (SiHa) and normal cell line (3T3-L1) along with intracellular trafficking using different trackers. **a)** The relative number density of cells following treatment is shown in fluorescent microscopic images of AO/EtBr staining of control, doxorubicin (DOX, pH~7-8), DOX loaded LDHs (DOX@LDH1 and DOX@LDH3) with the concentration of 20 µg/ml. Scale Bar: 45 µm; **b)** MTT assay-based cell viability analysis of DOX, DOX@LDH1 and DOX@LDH3 against SiHa cells line with concentration 20 µg/ml; **c)** DOX, DOX@LDH1 and DOX@LDH3 groups (20 µg/ml) *in vitro* cytotoxicity in 3T3-L1 fibroblast cells at various incubation time intervals: results are shown in mean value ±SD, n = 3, \*\*\* p < 0.001, \*\* p < 0.01, \* p < 0.05; and **d)** Microscopic images of SiHa cells which has been stained with 100 nM LysoTracker green and 5 µg/ml DAPI after being exposed to DOX@LDH3 (20 µg/mL) for indicated time periods. Magnification: 40x ..... 131

**Figure 3.8:** *In vitro* cellular characterization of DOX loaded Li-Al based LDHs nanoformulations, capacity on uptake and adherence properties in cancer cell line (SiHa); **a)** Fluorescence microscopic images demonstrating how SiHa cells ingest DOX loaded LDH1 and LDH3 (DOX@LDH1 and DOX@LDH3) with time. LDH does not exhibit any fluorescence. Depending on cellular absorption, cells are exposed to 20 µg/ml DOX, pristine LDH (LDH3) and DOX loaded nanoformulations that exhibit varying fluorescence intensities. Magnification: 40x; **b)** Cellular uptake kinetics analysis using SiHa cells under various incubation periods. DOX was penetrated into the cells in the presence of DOX@LDH1 / DOX@LDH3 with equivalent DOX concentration of 20 µg/ml; **c)** Phase contrast images of the SiHa cells grown on the indicated substrates after 24 hours of incubation, scale bar: 48 µm; and **d)** The relative cell adhesion values after 24 hours of incubation using the designed indicated nanoformulations.....134

**Figure 3.9:** *In vitro* evaluation on the antitumor effect of the designed nanoformulations. **a)** Cell cycles were arrested following the treatment with three distinct chemotherapeutic agents. SiHa cells were either left untreated (control), or were given DOX, DOX@LDH1 and DOX@LDH3 (20 µg/ml) for 24 hours. The cells were fixed and stained with propidium iodide to detect DNA. The percentages of cells in G1, S, and G2/M states were determined using CytExpert Software; **b)** SiHa cells exposed to DOX, DOX@LDH1 and DOX@LDH3 had their annexin V and propidium iodide staining examined through flow cytometry. Control and three groups (20 µg/ml) were administered to cells for 24 hours. Propidium iodide (PI) labelled population is stained on the y-axis while Annexin V-FITC binding is seen on the x-axis. Viable cells are found in the lower left quadrant and are Annexin V negative and PI negative, early apoptotic cells are found in the lower right quadrant and are Annexin V positive and PI negative, and necrotic and late apoptotic cells are found in the upper left and right quadrant, respectively; **c)** The suggested molecular mechanism for the apoptotic cell death caused by nanoformulation; and **d)** Western blot analysis of SiHa cells after the treatment of PBS (I), DOX (II), DOX@LDH1 (III) and DOX@LDH3 (IV) (20 µg/ml) for 24 h, to determine the expression of Pro-caspase 3, BCL-XL, p53 and PARP proteins. Proteins from cell lysates were produced, separated on SDS-polyacrylamide gel, and then transferred to nitrocellulose membranes. The indicated antibodies were used to probe the membranes. Protein loading was monitored using β-actin as control. The findings presented here arise from two or three separate investigations .....137

**Figure 3.10:** a) 3D view of receptor DNA topoisomerase II alpha. PDB (PROTEIN DATA BANK) ID-4FM9 (<https://www.rcsb.org/structure/4fm9>). The X-ray crystal structure DNA topoisomerase II alpha was retrieved from the RCSB PDB database. The obtained crystal structure of the receptor was prepared for receptor- ligand docking by following steps: water molecules, bound atoms were removed by using of widely used visualization tool- BIOVIA DISCOVERY STUDIO (2021). The energy was minimized by the PyRx software; **b)** Chemical structure of doxorubicin drug as a ligand The three dimensional (3D) structure of Doxorubicin retrieved from PubChem as SDF format; **c)** 3D view of Doxorubicin- DNA complex along with different type of interaction between ligand and receptor. The molecular docking of doxorubicin molecule with the receptor DNA topoisomerase II alpha was performed with the aid of PyRx software. After preparation of receptor (PDB ID-4FM9) and respective ligand (doxorubicin) molecule were uploaded on PyRx. After successful uploading, molecular docking has performed followed by the docking process of the software. After completion of docking process best docking results has obtained which pose in the receptor cavities.....139

**Figure 3.11:** *In vivo* therapeutic efficacy of the nanoformulation using melanoma bearing mice. **a)** Schematic illustration of apoptosis based therapeutic action of DOX@LDH3-MC. The injectable hydrogel was injected just below the tumor site, DOX would be accumulated in tumor tissues due to the enhanced permeability and retention effect; **b)** Images taken of the tumor size in mice before and after treatments with DOX-MC (DOX in MC gel), DOX@LDH3-MC (DOX embedded in LDH3 and further embedded in MC gel), and control (only saline); **c)** Measured tumor volume as a function of time following the therapy with various approaches, as appropriate; **d)** Percentage of relative body weight as a function of treatment time in each group; **e)** Following intravenous administration of either pure DOX (5 mg/kg of mice weight) or DOX intercalated LDH1 and LDH3 (DOX@LDH1 and DOX@LDH3) with an equivalent quantity of drug in dispersion condition, the drug concentration profile in plasma was determined as a function of time. The dotted line represents the minimum inhibitory concentration (MIC) of DOX for *Mycobacterium smegmatis* ( $M_{sm}$ ); and **f)** The concentration of DOX in tumor tissue and different organs from melanoma tumor-bearing mice treated with DOX-MC or DOX@LDH3-MC at a dose of 5 mg/kg after 72 hours of injection.....143

**Figure 3.12:** *In vivo* therapeutic efficacy of the nanoformulation using melanoma bearing mice. **a)** Schematic illustration of apoptosis based therapeutic action of DOX@LDH3-MC. The injectable hydrogel was injected just below the tumor site, DOX would be accumulated in tumor tissues due to the enhanced permeability and retention effect; **b)** Images taken of the tumor size in mice before and after treatments with DOX-MC (DOX in MC gel), DOX@LDH3-MC (DOX embedded in LDH3 and further embedded in MC gel), and control (only saline); **c)** Measured tumor volume as a function of time following the therapy with various approaches, as appropriate; **d)** Percentage of relative body weight as a function of treatment time in each group; **e)** Following intravenous administration of either pure DOX (5 mg/kg of mice weight) or DOX intercalated LDH1 and LDH3 (DOX@LDH1 and DOX@LDH3) with an equivalent quantity of drug in dispersion condition, the drug concentration profile in plasma was determined as a function of time. The dotted line represents the minimum inhibitory concentration (MIC) of DOX for *Mycobacterium smegmatis* ( $M_{sm}$ ); and **f)** The concentration of DOX in tumor tissue and different organs from melanoma tumor-bearing mice treated with DOX-MC or DOX@LDH3-MC at a dose of 5 mg/kg after 72 hours of injection.....146

**Figure 4.1:** Evaluation of polymeric chain interactions and grafting with Li-Al based layered double hydroxide nanocomposite. **a)** The  $^1\text{H}$  NMR spectra of polyurethane prepolymer (P), and grafted derivative (P-L) reveal significant changes in hydrogen bonding, and the emergence of a new peak, at 9.9 ppm indicating successful grafting; **b)** The  $^{13}\text{C}$  NMR spectra of P and P-L of the grafted counterparts further confirm the graft reaction with the appearance of a distinct new peak, additional detailed NMR peak information can be found in the Supplementary Information; **c)** FTIR spectra of the prepolymer (P) and graft nanocomposite (P-L) exhibit shifts in peak positions, underscoring the molecular interactions involved in the grafting process. In the FTIR spectrum, a distinct inset plot showcases the wavenumber range between 4000 and 3000  $\text{cm}^{-1}$ , clearly highlighting the successful grafting of the chemical reaction between polyurethane and the Li-Al-based LDH nanocarrier (L). This interaction signifies the formation of a novel nanocomposite (P-L), demonstrating the effectiveness of the process; **d)** In comparison illustration of the solid state UV-Vis spectra of the prepolymer (P) and nanocomposite (P-L) that are indicated; **e)** Comparative X-ray diffraction analysis of prepolymer and nanocomposite (P-L); **f)** The DSC thermograms for P and P-L show the values for the melting point and heat of fusion, **g)** TGA thermograms demonstrating the relative temperature stability of prepolymer (P) and novel grafting nanocomposite.....170

**Figure 4.2:** **a)** Uv-Vis spectra pure Dox, Dox loaded P and Dox loaded P-L. **b)** FTIR spectra pure Dox, Dox loaded P and Dox loaded P-L. **c)** X-ray diffraction analysis of Dox loaded P and Dox loaded P-L. **d)** The DSC thermograms for Dox loaded P and Dox loaded P-L.....173

**Figure 4.3:** Polyurethane prepolymer grafted Li-Al based layered double hydroxide nanocomposite (P-L) morphological behaviour, **a)** HRTEM microscopic image of P-L; **b)** HRSEM images of nanocomposite P-L; **c)** AFM images in semi-contact mode ( $5 \times 5 \mu\text{m}^2$ ) of P-L nanocomposite, **d)** Greater agglomerates can be seen in the nanocomposite (P-L) optical picture.....176

**Figure 4.4** Some important characteristics of the designed nanocomposite include: **a)** Stress-strain charts illustrating the strengths of distinct nanocomposites, specifically polyurethane prepolymer grafted with Li-Al based layered double hydroxide, referred to as P-L (chemical). The comparative stress-strain curves are shown in the inset graph for polyurethane prepolymer (P), Li-Al based LDH nanocarrier physically mixed with prepolymer, designated P-L (Physical), and when 2-butanol chemically reacts with polyurethane prepolymer (REF); **b)** Schematic illustration comparing P-L (Chemical) and P-L (Physical): Understanding the Dynamics Behind the Stress-Strain Curves. The stress-strain curves of P-L (Chemical) and P-L (Physical) reveal essential material responses under tension, showcasing a remarkable contrast in behavior. P-L (Chemical), driven by strong covalent cross-linking, effectively absorbs and dissipates energy, resulting in a stress-strain curve that stretches far beyond conventional expectations. This increased elasticity and resilience yield an extraordinary strain percentage, reflecting the material's ability to deform significantly without fracture, showcasing its tenacity under stress. Conversely, P-L (Physical), while resilient, derives its strength from weaker, reversible interactions such as hydrogen bonds or van der Waals forces. As observed in polyurethane prepolymer, these physical cross-links demonstrate a more limited deformation before yielding to stress, resulting in a controlled stress-strain curve with lower strain values. The difference in strain extent between these two systems lies in the bonding nature: P-L (Chemical) exhibits a passionate, nearly limitless stretch, while P-L (Physical) reflects a more restrained, practical performance. This fundamental divergence illustrates why P-L (Chemical) is distinguished by its remarkable strain capacity, while P-L (Physical), although stable, remains conservative in its elastic limits. **c)** Rheological insights into polyurethane prepolymer (P) and the prepolymer-grafted Li-Al layered double hydroxide nanocomposite (P-L) at 160°C. At the elevated temperature of 160°C, the rheological behavior of polyurethane prepolymer (P) and its nanocomposite counterpart, where Li-Al based layered double hydroxide is grafted onto the prepolymer matrix (P-L)(Fig 4.4.c),

reveals a complex interaction of molecular dynamics. The heat activates polymer chain mobility in the prepolymer (P), facilitating a deeper exploration of its viscoelastic properties, such as shear thinning, relaxation, and flow characteristics. Meanwhile, the presence of the Li-Al nanofiller within the composite (P-L) enhances mechanical strength and thermal stability by introducing a hybrid nanostructure that resists deformation. The synergy between the polymer matrix and the layered double hydroxide at this temperature unveils a fascinating realm of tunable viscoelasticity, viscosity reduction, and improved mechanical performance, presenting potential for advanced materials engineering. **d)** Understanding Dynamic Mechanical Analysis (DMA) of the novel nanocomposite (P-L) and its glass transition temperature. Dynamic Mechanical Analysis (DMA) serves as a crucial tool in revealing the complex mechanical behaviour of materials, particularly in nanocomposites. In studying the novel nanocomposite (P-L), DMA provides significant insights into its viscoelastic properties, illuminating the material's response to stress, strain, and frequency variations across a temperature range. One of the most critical revelations from DMA is the glass transition temperature (T<sub>g</sub>) of the nanocomposite. This temperature marks a crucial threshold where the material transitions from a rigid, glassy state to a more flexible, rubbery phase. For (P-L), understanding this shift reveals not only its thermal stability but also its potential for various applications where mechanical resilience and adaptability are essential. The T<sub>g</sub> signifies the onset of molecular motion within the matrix, with the nanoscale reinforcements in (P-L) playing a vital role in modulating this behaviour.....180

**Figure 4.5:** a) FTIR spectra of P-L chemical ,P-L (physical) and pure P. b) UV-VIS spectra of P-L chemical ,P-L (physical) and pure P. c)Stress strain plot of of P-L chemical ,P-L (physical) and pure P. d)Mechanical parameters of P-L chemical ,P-L (physical) , pure P and reference molecule.....183

**Figure 4.6:** Temperature modulated Rheological behaviour of P and P-L .....185

**Figure 4.7:** The pH-triggered drug release from the formulation is governed by robust interactions between doxorubicin (Dox) and prepolymer grafted Li-Al layered double hydroxide (LDH) nanocomposites, ensuring a thermodynamically regulated, controlled, and sustained release.

**a)** A comparison of the cumulative drug release profiles for the prepolymer and grafted nanocomposite loaded with Dox (P@Dox and P-L@Dox) in PBS at 37 °C and approximately pH 7.4 shows that the stronger connections and larger confinement of the novel nanocomposite, P-L@Dox, facilitate continuous sustained drug release, whereas the prepolymer loaded Dox system (P@Dox) exhibits a burst release of the drug. **b)** Comparative release profiles of Dox in PBS at various pH levels (approximately 7.4, 6, and 4 at 37 °C) from the P-L@Dox formulation are illustrated. Data is presented as mean value ± SD (n = 3). **c)** A schematic illustration depicts the mechanism of medication release from the designed nanocomposite architecture. **d)** The configuration of interactions between the Dox molecule and the prepolymer grafted Li-Al based LDH nanocomposite, highlighting the corresponding hydrogen bonding. **e)** Variation in the total energy of all components involved in the design of the nanocomposite and the novel formulation is presented, with color coding: blue for Aluminum, green for Lithium, red for Oxygen, white for Hydrogen, and black for Carbon. **f)** The interaction energy variations for the LDH+Dox, LDH+P, and LDH+P+Dox systems are analyzed to understand the thermodynamic efficiency and potential for formulating effective nanocomposites.....188

**Fig 4.8.** Different kinetic model of controlled drug release ..a)Zero order Model, b)First order model,c)Korsmeyer- Peppas Model. d) Higuchi model.....190

**Figure 5.1:** **a)** Fluorescent microscopic images of AO/ EtBr staining of Control, P-L and P ; **b)** Cell viability study of Control, P-L and P against SiHa cells using MTT assay as a function of time; **c)** Cell viability of Control, P-L and P against 3T3-L1 using MTT assay as a function of time **d)** Phase contrast images of Control, P-L and P ; **e)** Percentage cell adhesion value of Control, P-L and P.....210

**Figure 5.2:** Comparative analysis of biocompatibility and *in vitro* cytotoxicity along with intracellular trafficking utilizing several trackers on the cancer cell line SiHa and the normal cell line 3T3-L1. **a)** MTT assay-based cell viability analysis of Dox, P@Dox and P-L@Dox against SiHa cells line at concentration 20 µg/ml; **b)** Fluorescence microscopy images of AO/EtBr staining of control, doxorubicin (Dox, pH~7-8), P@Dox and P-L@Dox at a concentration of 20 µg/ml reveal the relative number density of cells after treatment. **Scale bar: 50 µm and magnification:40x;**

c) *In vitro* cytotoxicity of Dox, P@Dox and P-L@Dox groups (20 µg/ml) in 3T3-L1 fibroblast cells at different incubation time intervals: results are shown in mean value ±SD, n = 3, \*\*\* p < 0.001, \*\* p < 0.01, \* p < 0.05; and d) Microscopic images of SiHa cells that have been stained with 100 nM LysoTracker green and 5 µg/ml DAPI after being exposed to P-L@Dox in different time periods, **Scale bar: 50 µm and magnification:40x**.....211

**Figure 5.3:** Dox-loaded prepolymer and prepolymer grafted Li-Al based LDH formulations: *in vitro* cellular characterization, capacity on uptake along with adhesion qualities in cancer cell line, SiHa. **a)** Fluorescence microscopy pictures showing the gradual uptake of Dox loaded P and L-P (P@Dox and P-L@Dox, respectively) by SiHa cells. Cells are subjected to 20 µg/ml Dox, P@Dox and P-L@Dox with different fluorescence intensities, depending on cellular absorption. **40x magnification and a 50 µm scale bar;** **b)** Analysis of the cellular uptake kinetics with SiHa cells under varied incubation times of P@Dox / P-L@Dox with equivalent Dox concentration of 20 µg/ml; **c)** The percentage cell adhesion values using the designed indicated nanoformulations after 24 hours of incubation for Dox was penetrated into the cells in the presence of P@Dox / P-L@Dox with equivalent Dox concentration of 20 µg/ml; **d)** Phase contrast images of the SiHa cells grown on the indicated substrates after 24 hours of incubation, **40x magnification and a 50 µm scale bar** of P@Dox / P-L@Dox with equivalent Dox concentration of 20 µg/m.....214

**Figure 5.4:** Assessment of the anticancer impact of the designed novel formulations (P-L@Dox) as compared to the traditional anticancer drug doxorubicin (Dox) for *in vitro* analysis. **a)** Using FACS study, the staining of SiHa cells exposed to P-L, Dox and P-L@Dox was evaluated for annexin V and propidium iodide. Cells were treated with designed nanocomposite and other two groups (20 µg/ml) for a 72 hrs. On the y-axis, the population tagged with propidium iodide (PI) is stained, and on the x-axis, Annexin V-FITC binding is visible. Necrotic and late apoptotic cells are located in the upper left (Q1) and right (Q2) quadrants, respectively; viable cells are found in the lower left (Q3) quadrant and are Annexin V negative and PI negative; early apoptotic cells are found in the lower right (Q4) quadrant and are Annexin V positive and PI negative; **b)** After being treated with different chemotherapeutic drugs, cell cycles were stopped. SiHa cells were either treated with nanocomposite P-L, traditional anticancer drug Dox and designed formulation P-L@Dox (20 µg/ml) for a 72 hrs. To find DNA, the cells were fixed and stained with propidium iodide and the percentages of cells in the G0/G1, S, and G2/M states were calculated;

c) SiHa cells were treated with 20 µg/ml of material (P-L), doxorubicin drug (Dox) and design formulation (P-L@Dox) for 72 hours. The expression of caspase 3, Bax, Cleaved caspase 9, Bcl2, p53, and PARP proteins were assessed by Western blot analysis; d) The relative expression of the specified protein markers has been meticulously quantified through western blot analysis; e) The relative expression levels of mRNA for p53, Bax, PUMA, and Bcl-2 were quantitatively assessed through a detailed RT-PCR analysis; f) Photographic images of the colony study for Material, Dox, and P-L@Dox were captured after 72 hours of incubation for each sample, using a concentration of 20 µg/ml; g) Plot of number of colonies for material P-L, drug Dox and formulation P-L@Dox reflecting the potent efficacy towards cancer of the designed formulation; h) Microscopic images capturing the migration of SiHa cancer cells treated with material P-L, Doxorubicin Dox, and a specially designed formulation P-L@Dox after 72 hours incubation with samples concentration 20 µg/ml reveal striking evidence of enhanced efficacy. These images illustrate the profound impact of the treatment, showcasing a higher rate of apoptosis, as the cancer cells are visibly impaired in their movement, a testament to the potent therapeutic action of the formulation; i) The bar diagram illustrating the wound area across different groups such as, material P-L, Dox, and our designed formulation P-L@Dox elegantly reveals the potent efficacy of our novel formulation against cancer. The clear distinction between the groups highlights the remarkable impact of our formulation, emphasizing its therapeutic potential in comparison to the others. .... 217

**Figure 5.5:** The effectiveness of the injectable formulation (P-L@Dox-MC) for *in vivo* therapy in mice with melanoma that contain luciferase. **a)** Images capturing the tumor sizes in mice, both before and after treatments, reveal the effects of various interventions. The treatments include Dox-MC (Dox encapsulated within an MC gel), P-L@Dox-MC (Dox incorporated into P-L, further embedded in an MC gel), and a control group receiving only saline. These visual comparisons offer a glimpse into the transformative impact of each treatment, providing a clear distinction between the progression or regression of tumors across the experiment; **b)** Photographic images showcasing the measured tumor volumes, accompanied by a scale, were captured after treatment across various groups i.e. Control, Dox-MC and P-L@Dox-MC. At the conclusion of the 22-day experiment, tumors from the different groups of animals were carefully collected and measured; **c)** Measured tumor volume over time as influenced by the therapy, with different approaches applied where appropriate, **d)** Percentage of relative body weight as a function of treatment time across all groups;

e) After intravenous administration of either pure Dox (5 mg/kg of mouse body weight) or Dox intercalated within polyurethane prepolymer grafted Li-Al based layered double hydroxide nanocomposite (P-L@Dox), containing an equivalent dose of the drug in dispersion form, the drug concentration profile in plasma was measured over time. The dotted line on the graph denotes the minimum inhibitory concentration (MIC) of DOX against *Mycobacterium smegmatis* (Msm); f) The levels of doxorubicin (Dox) in tumor tissue and various organs were assessed in melanoma tumor-bearing mice following treatment with Dox-MC and P-L@Dox-MC. This evaluation took place 72 hours after administering a dosage of 5 mg/kg; g) A Comprehensive study of bioluminescence in luciferase-expressing B16-F10 melanoma-bearing mice across three different groups over time.. ..... 222

**Figure 5.6:** : Examining the Complex Effects of *In Vivo* Controlled Drug Release on Melanoma Tumor Tissues and Various Organs, Accompanied by Comprehensive Biochemical Assays a) Tumor tissues from mice across different treatment groups were carefully excised after 22 days of treatment and subjected to histopathological examination using H&E staining at a magnification of 40x. b) Following the same treatment duration, vital organs, including the liver, kidneys, spleen, and lungs, were collected from the mice and analyzed histopathologically with H&E staining at 40x magnification. c) The immunohistochemical analysis of tumor tissues at the end of the treatment revealed detailed expressions of the inflammatory marker TNF- $\alpha$  and the vascular differentiation marker CD31, observed at a magnification of 40x. d) Liver function tests were conducted by analyzing serum levels of AST, ALT, and ALP across different treatment groups, providing insights into hepatic health and functionality. e) Serum levels of BUN and creatinine were carefully assessed across the various therapy groups as part of a comprehensive renal function test, with arrows indicating values corresponding to healthy mice as a benchmark for renal health.....237



## *List of Tables*

**Table 3.1:** Proposed general formula of  $M^{1+}/M^{3+}$  type LDHs which can be justified by theoretically, where  $x$  is the cation substitution ratio (evaluated from XPS analysis),  $m$  is the number of anionic charge and  $n$  is the number of entrapped water molecule. In this work, by varying the Li and Al elements, we mainly synthesize three nanocarriers (detailed discussed in synthesise section) named LDH1, LDH2 and LDH3. From LDH1 to LDH3, we gradually increase in aluminum concentration which can be justified by all elemental characterizations such as HRSEM and XPS analysis. The value of cation substitutions ratio ( $x$ ) of LDH1, LDH2 and LDH3 are 0.64, 0.67 and 0.75 respectively. Here we mention the chemical formula of LDH1, LDH2 and LDH3 by using XPS analysis along with maintaining the charge balance.....113

**Table 3.2** Molecular docking analysis to determine the binding sites, interacting hydrogen and oxygen bonds, amino acid residues and atoms. PyRx was used for calculating the docking score and root mean square deviation (RMSD) values of interacting molecules. The binding site and interaction were visualized by virtual screening tool Pymol software. Using Pymol software; bonds, distance between bonds, and interacting amino acid/ nucleotides residues were estimated for ligand molecule. Receptor- ligand interaction and generation of images were rendered using Pymol AND BIOVIA DISCOVERY STUDIO-2021 (DeLano, 2002). The best-suited conformations with the lowest root mean square deviation (RMSD) values, highest docking score, and number of amino acids residues with binding H and O bonds were collected.....141



# *List of Schemes*

<b>Scheme 4.1</b> Synthetic Scheme of PU grafted LDH (P-L).....	166
---	-----



## *Abbreviations*

<b>DSC</b>	Differential Scanning Calorimetry
<b>FTIR</b>	Fourier Transformation Infrared
<b>h</b>	Hour
<b>LDH</b>	Layered Double Hydroxide
<b>MTT</b>	4, 5- dimethylthiazole-2yl-2, 5- Diphenyltetrazolium Bromide
<b>°C</b>	Degree Centigrade
<b>SEM</b>	Scanning Electron Microscope
<b>t</b>	Time
<b>T</b>	Temperature
<b>TEM</b>	Transition Electron Microscope
<b>TGA</b>	Thermal gravimetric Analysis
<b>UTM</b>	Universal Testing Machine
<b>XRD</b>	X-ray diffraction
<b>DFT</b>	Density function

